2.2 SAR Interferometry

This section reviews the history, definitions and configurations of SAR interferometry for various applications such as topographic mapping, surface displacement measurement, and the surface random change detection.

2.2.1 History of InSAR

SAR interferometry was first used in observation of the surface of Venus and the Moon from InSAR configurations using antennas on the Earth's surface (Rogers and Ingalls, 1969). Graham (1974) was the first to introduce synthetic aperture radar for topographic mapping. Zebker and Goldstein (1986) presented the first practical results of observations with airborne radar. Goldstein *et al.* (1988) was the first to apply InSAR technique to the spaceborne observations to generate highly accurate digital elevation model (DEM) of the Earth's surface using the SEASAT-A L-band SAR system. With the launch of ERS-1 (1991), JERS-1 (1992), and RADARSAT (1995), spaceborne InSAR study has increased dramatically. With the launch of ERS-2 in 1995, the feasibility of spaceborne SAR interferometry has been greatly improved by the use of ERS-1 and ERS-2 in the tandem mission that can provide interferometric data at only one-day separation (Duchossois and Martin, 1995).

Technical refinement of InSAR for DEM generation can be found in Madsen *et al.* (1993) and Zebker *et al.* (1994b). The concept of DInSAR was established by Gabriel *et* *al.* (1989). Massonnet *et al.* (1993) used a pre-existing DEM to remove the topographic phase from interferogram and retrieved the co-seismic displacement field of the Landers earthquake in California. Zebker *et al.* (1994a) used three-pass DInSAR configurations to remove directly the topographic phase without use of the reference DEM. The use of coherence image for surface stability study is a relatively recent study area in fast development (Massonnet *et al.*, 1995; Hagberg *et al.*, 1995; Rosen *et al.*, 1996; Liu *et al.*, 1997).

2.2.2 Definitions

The relatively recent and rapid development of SAR interferometry has created untidy and multiple definitions and nomenclatures used independently by different groups of scientists. A clear specific nomenclature for SAR interferometry is necessary for this thesis.

Interferometric SAR refers to a SAR system or configuration that incurs coherent correlation between multiple SAR observations of the same target. Several acronyms for interferometric SAR are used. These include InSAR, INSAR, IFSAR, or IfSAR, which are all equivalent. The term “InSAR” is used throughout this thesis. Note that InSAR normally refers to the across-track interferometric configuration rather than *along-track interferometer* (ATI) for moving target detection (Bao *et al.*, 1997; Carande, 1994) or Δk *-radar* for accurate range measurement using different wavelengths from the same antenna position (Sarabandi, 1997).

InSAR can be operated from either *airborne* or *spaceborne* platforms and configured for *single-pass* or *repeat-pass*. A single-pass interferometer is best for DEM generation while repeat-pass is essential for environmental change monitoring. Repeat-pass is only possible when vehicle revisit control is of high accuracy. An airborne system provides more flexible configuration and operation. However, an *airborne repeat-pass* interferometer is not operationally feasible at present because the motion and position control of aircraft is more difficult than spaceborne systems. An airborne interferometer is usually a single-pass configuration and has been widely used for DEM generation. Given accurate orbit control, *spaceborne repeat-pass* InSAR configuration for change detection of the Earth's surface is possible. A typical successful case is ERS-1 and ERS-2. SRTM is, so far, a unique example of a *spaceborne single-pass* interferometer.

SAR interferometry (equivalently, the InSAR technique) is a technique to extract surface physical properties by using the *complex correlation coefficient* of two SAR signals. The complex correlation coefficient, γ, of the two SAR observations, u_1 and u_2, is defined as:

$$\gamma = \frac{E[u_1 u_2^*]}{\sqrt{E[u_1 u_1^*]E[u_2 u_2^*]}} \tag{2.1}$$

where $E[]$ is the mathematical expectation (ensemble averaging) and $*$ represents the complex conjugate.

The *interferometric phase* is defined as the phase of the complex correlation coefficient as:

$$\phi = \arg\{\gamma\} = \arg\{E[u_1 u_2^*]\}, \tag{2.2}$$

and its two dimensional map is called the *interferogram.*

The *coherence* is the amplitude of the complex correlation coefficient as:

$$\rho = |\gamma|, \tag{2.3}$$

and its two dimensional map is called the *coherence image*.

An interferogram contains the interferometric phase fringes from SAR geometry, together with those from topography and displacement of the surface. The level of coherence can give a measure of the quality of the interferogram. Initially, the InSAR techniques were mainly dedicated to topographic information retrieval from interferograms. Further development resulted in techniques to extract interferometric phase fringes from coherent block displacement of the surface. This is called *differential SAR interferometry* (DInSAR). Coherence itself gives valuable information about the surface temporal stability. This is called *InSAR coherence imagery*, which is the main topic of this thesis.

2.2.3 Topographic Mapping

It is a consequence of SAR geometry that surface scatterers at the same distance from the radar (slant range) but with different look angles are imaged as the same point by SAR. SAR geometry provides only the slant range of the target but no information about its look angle. If this ambiguity of the radar look angle can be solved, the exact location (elevation and ground range) of each target point can be calculated. The look angle ambiguity in SAR geometry can be solved from the following InSAR geometry.

Consider a cross section of the Earth surface as shown in Figure 2.2. This figure is drawn in a plane perpendicular to the along-track direction. InSAR configuration is normally achieved by imaging a target point *P* from two radar positions at S_1 and S_2. The height of S_1 above zero elevation level is H. The radius of the Earth r_e, measured from the Earth's centre *O* to the datum, is assumed to be a constant along the across-track direction. This assumption usually holds for the case of a spaceborne SAR system with orbit inclination (the angle between the orbit plane and the Earth's equatorial plane) around 90° and having side-looking imaging property. The distance between S_1 and S_2 is called baseline, B. The angle of the baseline with respect to the horizon is β. The look angle is θ_l, and the slant ranges from S_1 and S_2 to the target points are R_1 and R_2, respectively. If the slant range difference is given by $\Delta R = R_2 - R_1$, then the measured interferometric phase is

$$\phi = -\frac{4\pi}{\lambda}\Delta R \tag{2.4}$$

This is 2π times the round-trip distance difference in wavelengths. By applying the law of cosines in ΔS_1PS_2, ΔR can be solved as

$$\Delta R = \sqrt{R_1^2 + B^2 - 2R_1B\sin(\theta_l - \beta)} - R_1 \tag{2.5}$$

From the measurement of the interferometric phase ϕ and InSAR geometric parameters, the look angle θ_l in equation 2.5 can be solved. Then, from ΔS_1OP, the topographic elevation *z* is calculated as

$$z = \sqrt{(r_e + H)^2 + R_1^2 - 2R_1(r_e + H)\cos\theta_l} - r_e, \tag{2.6}$$

and the ground range R_g is

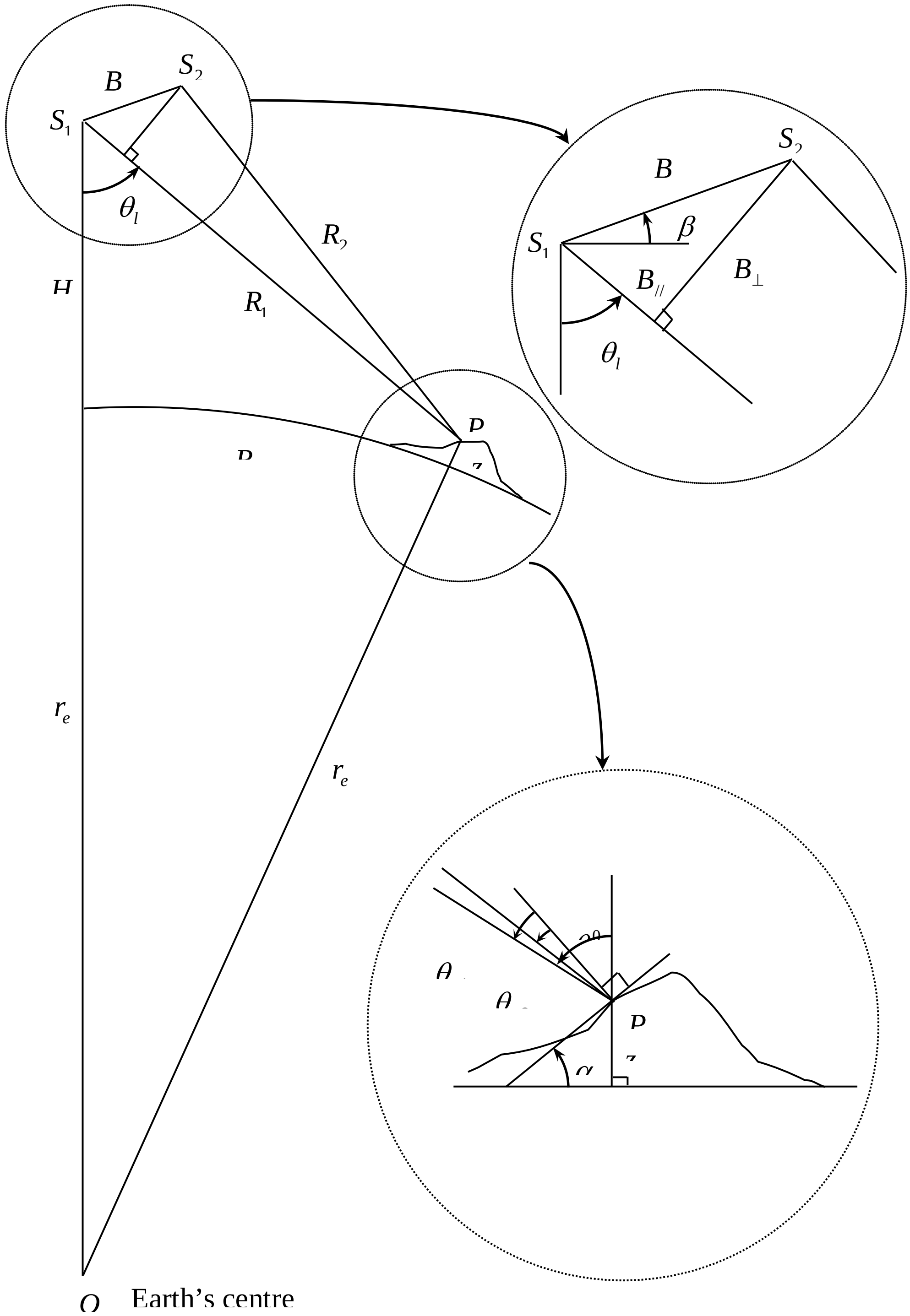

Figure 2.1 InSAR configuration.

$$R_g = r_e \sin^{-1}\left(\frac{R_1}{r_e + z} \sin\theta_l \right). \qquad (2.7)$$

From equations 2.4 and 2.6, the *height sensitivity* of InSAR, i.e., the amount of change in interferometric phase from the change of surface elevation, can be calculated as

$$\frac{\partial\phi}{\partial z} = \frac{4\pi}{\lambda} \frac{B\cos(\theta_l - \beta)}{R_1 \sin\theta_l} \cdot \left(\frac{R_1}{r_e + H} \cdot \frac{\sqrt{(r_e + H)^2 + R_1^2 - 2R_1(r_e + H)\cos\theta}}{\sqrt{R_1^2 + B^2 + 2R_1 B \sin(\theta_l - \beta)}} \right) \qquad (2.8)$$

Neglecting the minor term in brackets and using a parallel ray approximation (Zebker and Goldstein, 1986), the *height sensitivity* can be simplified as

$$\frac{\partial\phi}{\partial z} \approx \frac{4\pi}{\lambda} \frac{B_\perp}{R_1 \sin\theta_l} \qquad (2.9)$$

where $B_\perp$ is the baseline perpendicular component to the radar look direction while $B_{//}$ is the baseline parallel component, as depicted in Figure 2.2.

Alternatively, the *height of ambiguity* (Bamler and Hartl, 1998) is

$$z_{2\pi} = 2\pi \frac{\partial z}{\partial \phi} \approx \frac{\lambda}{2} \frac{R_1 \sin\theta_l}{B_\perp}, \qquad (2.10)$$

i.e., the height resulting in a phase change of one fringe (2π) characterises the resolution of topography derived from InSAR. From equations 2.9 and 2.10, it is obvious that a sufficiently large $B_\perp$ is necessary for accurate topography mapping. However, the $B_\perp$ value is limited in practice due to the spatial decorrelation that reduces the coherence level and the quality of the interferogram (Li and Goldstein, 1990).

Another important property of the interferogram is the *interferometric phase fringe number* in slant range, i.e., the number of interferometric phase (2π) fringes in slant range (Bamler and Hartl, 1998),

$$k_\phi = \frac{1}{2\pi}\frac{\partial \phi}{\partial R_1} \approx \frac{2B_\perp}{\lambda R_1 \tan(\theta_i^0 - \alpha)}, \tag{2.11}$$

where α is the surface slope measured positive towards the radar look direction, and θ_i^0 is the nominal incidence angle when $\alpha = 0\,°$. Alternatively, the *interferometric phase fringe frequency* in the range time (fast time) domain is given as (Gatelli *et al.*, 1994)

$$f_\phi = \frac{1}{2\pi}\frac{\partial \phi}{\partial t} \approx \frac{cB_\perp}{\lambda R \tan(\theta_i^0 - \alpha)} \tag{2.12}$$

by using the 2-way travel time relation, $2R = ct$.

2.2.4 Coherent Surface Displacement Measurement - DInSAR

The DInSAR technique gives the measurement of block displacement of land surface caused by subsidence, earthquake, glacier movement, volcano inflation, etc., to cm or even mm accuracy. If the surface displacement is as a result of single or cumulative surface movement occurred between the acquisition times of two SAR images S_1 and S_2, the component of surface displacement in the radar-look direction, ζ, contributes to additional interferometric phase as

$$\phi = \frac{4\pi}{\lambda}(\Delta R + \zeta) \tag{2.13}$$

For the purpose of surface displacement measurement, the zero-baseline InSAR configuration is the ideal as $\Delta R = 0$, so that

$$\phi = \phi_d = \frac{4\pi}{\lambda}\zeta \qquad (2.14)$$

This zero-baseline, repeat-pass InSAR configuration is hardly achievable in practice for either spaceborne or airborne SAR system. Therefore, a methodology to remove the topographic phase as well as the system geometric phase in a non-zero baseline interferogram is needed. If the interferometric phase from the InSAR system geometry and topography can be removed from the interferogram, the remnant phase would be the phase from block surface movement, providing that the surface maintains high coherence.

There are two DInSAR techniques to remove topographic phase from the interferogram: one is the DEM method (Massonnet *et al.*, 1993) and the other is the three-pass method (Zebker *et al.*, 1994). The first method uses a DEM generated from existing topographic information obtained from sources other than InSAR, such as a topographic map or stereo optical imagery. The topographic phase can then be calculated from the DEM and subtracted from the interferogram. The second method requires a reference interferogram, which is believed to contain the topographic phase only. The three-pass approach has the advantage in that all data structure is kept within the SAR data geometry while DEM method can produce errors by misregistration between SAR data and cartographic DEM. The three-pass approach is restricted by the data availability. The three-pass DInSAR technique is further discussed below.

The three-pass DInSAR technique uses another InSAR pair as a reference interferogram that does not contain any surface movement event as

$$\phi' = \frac{4\pi}{\lambda}\Delta R' \quad . \tag{2.15}$$

This motion-free interferogram can be achieved from short-revisit repeat-pass InSAR configuration or single-pass InSAR configuration. Strictly speaking, single-pass InSAR configuration is the only practical way to achieve motion-free interferogram where the motion is continuous such as ice sheets.

Incorporating equations 2.13 and 2.15 gives the phase difference, ϕ_d, only from the surface displacement as

$$\phi_d = \phi - \frac{\Delta R}{\Delta R'}\phi' = \frac{4\pi}{\lambda}\zeta \ . \tag{2.16}$$

In this processing, phase unwrapping must be applied to the reference interferogram. Phase unwrapping is one of the most challenging problems in InSAR technology, especially for low coherence areas. Several robust algorithms for phase unwrapping have been developed that are sufficient even for a highly mountainous area. The phase unwrapping algorithms will be discussed further in Chapter 7. For an exceptional case where $\frac{\Delta R}{\Delta R'}$ in equation 2.16 is a positive integer number, phase unwrapping may not be necessary (Massonnet *et al.*, 1996). However, this situation is not realistic and it is very hard to achieve from the system design for a repeat-pass interferometer.

From equation 2.16, the *displacement sensitivity* of DInSAR is given as

$$\frac{\partial \phi_d}{\partial \zeta} = \frac{4\pi}{\lambda} . \tag{2.17}$$

Comparing with height sensitivity of InSAR in equation 2.9, interferometric phase is much more sensitive to surface geometric change than to topography. Therefore, DInSAR technique can measure surface displacement to centimetre or millimetre level while InSAR measures topography to an accuracy of no better than several metres.

The applications of DInSAR have been successful in measurement of glacier and ice sheet dynamics (Fahnestock *et al.*, 1993; Goldstein *et al.*, 1993; Hartl *et al.*, 1994; Joughin *et al.*, 1995; Kwock and Fehnestock, 1996; Thiel *et al.*, 1995; Thiel and Wu, 1996; Wu *et al.*, 1997), seismic deformations (Feigl *et al.*, 1995; Massonnet and Feigl, 1995; Massonnet *et al.*, 1993, 1996a; Meyer *et al.*, 1996; Reigber *et al.*, 1997; Zebker *et al.*, 1994a), volcanic activities (Briole *et al.*, 1997; Massonnet *et al.*, 1995; Roth *et al.*, 1997; Thiel *et al.*, 1997), and land subsidence (Liu *et al.*, 1999c; Massonnet *et al.*, 1997; Raymond and Rudant, 1997).

2.2.5 Random Surface Change Detection – InSAR Coherence Imagery

The coherence of two SAR observations represents the similarity of the radar reflection between them. The main purpose of InSAR coherence imagery is to detect and monitor surface random change processes. If the reflection or dielectric property of a target has been changed during the observation time interval, the coherence of that target is reduced so that it appears dark in the coherence image.

The coherence image of two time-separated SAR observations provides an automatic detection of the random change of the target surface. Unstable and changing ground objects, which are detectable using InSAR coherence imagery, include lakes, rivers, crop fields, vegetation, surface erosion, sand transformation, and activities of living creatures. Several successful applications have been published describing land cover classification and random change detection in forest canopy (Askne and Hagberg, 1993; Askne *et al.*, 1997; Borgeaud and Wegmuller, 1996; Wegmuller and Werner, 1997; Wegmuller *et al.*, 1995), sand encroachment (Liu *et al.*, 1997, 1999a), rapid erosion (Liu *et al.*, 1999b, 1999d), and for seismic hazard mapping (Ito *et al.*, 2000).

3.3 InSAR Coherence Image Generation

From the two coregistered SLCs, an interferogram can be generated by calculating the phase difference of two signals pixel by pixel. This “raw” interferogram with a non-zero baseline contains phase fringes mainly from the system geometry and topography. The system geometric phase fringes and the spatial decorrelation factor from local slope variation should be removed so that only the temporal decorrelation can be evaluated from the level of coherence.

The general data processing procedures for coherence map generation are as follows. First, the system geometric phase is removed using the *Earth flattening* procedure. The remnant phase fringes can be assumed as those from topography. The topographic phase fringe number is calculated to determine the parameters for range spectral filtering for local slope variation to compensate the decorrelation from range spectral misalignment.

The following sections describe in detail the processing for InSAR coherence image generation

3.3.1 Earth Flattening - System Geometric Phase (ϕ_0) Removal

The *system geometric phase fringe number* in slant range can be calculated from equation 2.11 when $\alpha = 0^\circ$ as

$$k_{\phi_0} = \frac{2B_\perp}{\lambda R \tan\theta_i^0}. \tag{3.1}$$

The fringe number from InSAR geometry ϕ_0 is strongly dependent on the baseline perpendicular component $B_\perp$. The removal of this phase is essential for coherence estimation especially when the InSAR image pair was configured with a large enough baseline to produce sufficient height sensitivity for topographic mapping.

When sufficiently accurate system and orbit data are available, which is generally true for ERS-1/2, Earth-flattening is a relatively easy task. Since the orbit state vectors containing the position and velocity information of the satellite are sparsely time sampled, an orbit propagator program, such as “getorb” of Delft Institute for Earth-Oriented Space Research (DEOS), is necessary to obtain the precise orbit parameters for the scene (Scharroo and Visser, 1998).

The system geometric phase can be compensated by considering the elliptical earth surface (e.g. WGS84) where the surface elevation is zero ($z = 0$). The look angle on zero-elevation surface, θ_l^0, is determined from the geometric relations $\Delta S_1 OP$ in Figure 2.3 as

$$\theta_l^0 = \cos^{-1}\left(\frac{R_1^2 + (r_e + H)^2 - r_e^2}{R_1 (r_e + H)} \right), \tag{3.2}$$

then the phase difference from the system geometric phase is determined as

$$\phi_0 = \frac{4\pi}{\lambda} \Delta R\big|_{z=0}, \tag{3.3}$$

where

$$\Delta R\big|_{z=0} = \sqrt{R_1^{\,2} + B^2 + 2R_1 B \sin(\theta_l^0 - \beta)} - R_1 . \tag{3.4}$$

The system geometric phase ϕ_0 is then removed from the interferogram to give the Earth-flattened interferogram,

$$\phi_{flat} = \phi - \phi_0 . \qquad (3.5)$$

3.3.2 Range-varying Spectral Filtering

To compensate for the spatial baseline decorrelation from range spectral misalignment, the flat-earth approximation, applied in range spectral filtering (section 3.2.1), is not sufficient and the range-varying filter must be used to incorporate the local topographic variation. Although the spectral misalignment is a function of the local slope (equation 2.55), knowledge of the local slope information is not necessary *a priori* in this processing. The reason for this is that the amount of range spectral misalignment ν_0, given in equation 2.55, is equivalent to the interferometric phase fringe frequency f_ϕ in equation 2.12. The estimation of the interferometric phase fringe frequency from the interferogram can therefore be used to design the range-varying spectral filter similar to equation 3.9. The bandwidths and central frequencies of the filter can be estimated from the fringes of interferogram after Earth-flattening.

3.3.3 Coherence Calculation

The coherence is the magnitude of the complex correlation coefficient calculated within an averaging window of the complex Earth-flattened interferogram as

$$\rho = \frac{\left| \sum_{l=1}^{L} |u_1(l)| |u_2^*(l)| e^{j\phi_{flat}} \right|}{\sqrt{\sum_{l=1}^{L} u_1(l) u_1^*(l)} \sqrt{\sum_{l=1}^{L} u_2(l) u_2^*(l)}}. \quad (3.6)$$

For unbiased coherence estimation, it should be assumed that the scene is locally stationary and ergodic within the averaging window. The size of the averaging window *L* is determined by a trade-off between unbiased coherence estimation and spatial resolution. Selecting a small averaging window ensures high spatial resolution, but may risk the bias of coherence estimation towards higher values especially in low coherence area (Touzi *et al.*, 1999). On the other hand, using a large averaging window may underestimate the coherence when the scene is inhomogeneous especially on steep slopes. These relations will also be further explained in Chapter 7.